Proceedings of the Canadian Society for Mechanical Engineering International Congress 2021
CSME Congress 2021
June 27-30, 2021, Charlottetown, PE, Canada

Effect of the Earth's Rotation on Hydraulic Jumps

1st Muveno Mucaza
Department of Mechanical and Materials Engineering
Western University
London, Canada
mmucaza@uwo.ca

2nd Kelly Anne Ogden
Department of Mechanical and Materials Engineering
Western University
London, Canada
kogden3@uwo.ca

***Abstract*—The influence of Earth's rotation on the structure and mixing of internal hydraulic jumps is studied by means of three-dimensional numerical simulations with varying values of the Coriolis parameter. The Navier-Stokes equations with vertical density stratification are solved numerically for an incompressible fluid. The flow structure varies across the width of the channel due to rotation. In particular, different jump structures are observed at positions across the width of the channel. Mixing also changes as a result of rotation, with larger mixing values occurring at lower rotation rates and on the left side of the channel (when looking in the direction of flow).**

***Index Terms*—internal hydraulic jump, Rossby radius of deformation, Coriolis parameter, rotation, mixing.**

I. Introduction

Hydraulic jumps are a phenomenon in which the depth of a layer of the flow changes suddenly, causing the flow to transition from supercritical ($Fr > 1$) to subcritical ($Fr < 1$), dissipating energy and converting part of the kinetic energy of the flow into potential energy. Because of their often highly turbulent and agitated nature, large eddies can form in the jump region that make hydraulic jumps very effective in dissipating mechanical energy and in mixing the fluids involved in such flows (an example being the introduction of air bubbles in open-channel flows with surface hydraulic jumps, or mixing fluid properties in internal hydraulic jumps). The occurrence of a hydraulic jump largely depends on the initial velocity of the flow; for subcritical flows, a jump would not occur, and as the velocity increases to supercritical with respect to the surface or interfacialinternal wave speeds, different types of waves and hydraulic jumps can be observed. Jumps may be held stationary by topography, or they might propagate, as in the case of a tidal bore [2]. Hydraulic jumps may exhibit various jump structures, such as a smooth undular (wave-like) jump, or a turbulent jump with overturns [8].

In open-channel flows, hydraulic jumps are prominent both at the free-surface and in the density interfaces of stratified fluids, called internal hydraulic jumps. Internal hydraulic jumps have been observed in nature both in open channels such as the Straight of Gibraltar, Knight Inlet, and Hood Canal [1], [5], [6], [11] and in compressible flows such as the flow past the Nevada mountain range where changes in properties such as transitions in pressure and potential temperatures were attributed to hydraulic jumps [15]. Several studies have predicted the factors that would lead to the formation of a turbulent hydraulic jump on a continuously stratified flow for a rigid bottom [14], [15] as well as flows over large amplitude topographies [13].

The theory of hydraulic jumps in the interior density surfaces of a stratified fluid has been discussed in previous papers using various two-layer approximation theories with shock-joining models to match upstream and downstream conditions [3], [4], [12]. These theories do not take into account the internal hydraulics of the jumps, and they use the principles of conservation of mass and momentum flux across the hydraulic jump; however, different theories arise as a consequence of assumptions made on how the energy loss is distributed between the layers. Wood and Simpson [3] proposed a model where energy conservation happened in the contracting layer, while Klemp et al [4] postulated that energy be conserved in the expanding layer. These theories were used by Ogden and Helfrich [8] to study the effect of upstream shear in flows with hydraulic jumps. Upstream shear becomes important in flows over topography, which is common in hydraulic jumps in the environment. Ogden and Helfrich [8] also present numerical simulations of the Navier-Stokes equations that account for non-hydrostatic processes, turbulence, and mixing in the transition from supercritical to subcritical flow. These simulations revealed that the different two-layer theories are suitable for different values of shear, and that strong mixing between the two layers, and entrainment in the case of jumps with large upstream shear, occurs, but is not captured by the theory [17].

Hydraulic jumps in continuously stratified flows have been studied observationally, for example by Gregg and Pratt [11], who reported on a possible jump in Hood Canal. They found hydraulic responses that resemble hydraulic jumps downstream of a prominent sill. Although their observations regarding a hydraulic jump in the lee of the sill in Hood Canal are not conclusive, Gregg and Pratt agree that more idealized simulations of Hood Canal that take into account the geometry of the topography and the time dependence are necessary for clarification. The effect of rotation is apparent in their observations, motivating the current study.

The effects of rotation in the formation of internal hydraulic jumps have been studied previously. Pratt *et al.* [10] considered

flow over a steady obstacle on an infinite, rotating channel where a hydraulic jump was found to have developed in both the depth and the stream width. They also observed that a jump formed that resembled a Kelvin wave, with it having a larger amplitude on the left-side wall and decaying along the width of the channel. Numerical simulations by Pratt [9] have also revealed a similar structure for a rotating hydraulic jump, with the amplitude of the jump changing over the width at an order of the global deformation radius. Although extensive studies have been done in rotational hydraulics, most of them focus on single layer flows. There is a need to expand the exiting knowledge of the internal hydraulics of continuously stratified flows to include the effects of rotation. This work investigates how Earth's rotation influences the structure and the mixing of internal hydraulic jumps in channel flows.

II. Governing Equations

The current work extends the study on non-rotating internal hydraulic jump in two-layer flows by Ogden and Helfrich [8] to investigate the effect of rotation. Ogden and Helfrich [8] compare the theoretical solution of hydraulic jumps with upstream shear to numerical results obtained from 2D and 3D simulations of an imposed hydraulic jump at the interface of a continuously stratified fluid. The simulations are three-dimensional and were conducted using the CFD code Gerris, with an isotropic grid composed of 128 points in the vertical direction.

Gerris is an open-source CFD tool that combines the use of quad/octree discretization, a multilevel Poisson solver used for solid boundaries in combination with a cell-merging technique for advection schemes, and a projection method used for uniform grids [16]. This tool was chosen for this work because it allows the meshing of complex boundaries, such as the existence of a topography at the bottom of the domain, by using mixed cells that are cut by the solid boundary [16]. This modelling tool is used to solve the incompressible Navier-Stokes equations applied to the motion of a thin layer of fluid on the rotating earth. The Boussinesq approximation is also used for the density stratification of the fluid. The governing equations are

$$\nabla \cdot \boldsymbol{u} = 0, \tag{1}$$

$$\frac{\partial \mathbf{u}}{\partial t} + \mathbf{u} \cdot \nabla \mathbf{u} = -\frac{1}{\rho_0} \nabla p + \nu \nabla^2 \mathbf{u} + \frac{g(\rho - \rho_0)}{\rho_0} \mathbf{k} - 2\boldsymbol{\Omega} \times \mathbf{u}, \tag{2}$$

$$\frac{\partial \rho}{\partial t} + \mathbf{u} \cdot \nabla \rho = \kappa \nabla \rho, \tag{3}$$

The velocity vector $\mathbf{u}$ is broken into the cartesian components u in the allong channel direction, v in the transverse direction, and w in the vertical direction. The expression $\frac{g(\rho-\rho_0)}{\rho_0}$ is the reduced gravity g' and κ is the density diffusivity.

The Coriolis force can be expressed in terms of the Coriolis parameter f as

$$(2\boldsymbol{\Omega} \times \mathbf{u})_x = -(2\Omega sin(\theta))v = -fv \tag{4}$$

$$(2\boldsymbol{\Omega} \times \mathbf{u})_y = (2\Omega sin(\theta))u = -fu \tag{5}$$

$$(2\boldsymbol{\Omega} \times \mathbf{u})_z = -(2\Omega cos(\theta))u \tag{6}$$

with the Coriolis force in the z-direction assumed to be negligible when compared to the other terms in the right hand side of the z-momentum equation.

The effects of rotation in the flow are determined by the rotation parameter f and the width of the channel when compared to the Rossby radius of rotation, which defines the width at which rotational effects are relevant when compared to buoyancy effects. For a continuously stratified medium, the Rossby radius is given by

$$L_{R,n} = \frac{NH}{n\pi f_0}, \tag{7}$$

where H is the lengthscale, n is the mode of the jump (with mode one jumps being the primary focus of this work), and N is the Brunt-Väisälä, or buoyancy, frequency and is given by

$$N^2 = -\frac{g}{\rho_0}\frac{d\rho}{dz}, \tag{8}$$

and it describes the frequency at which a displaced parcel of fluid would oscillate in the vertical direction in a stratified fluid.

Considering the flow's domain, the expression $d\rho$ becomes $(\rho_{max} - \rho_{min})$, and dz is the height of the domain H. This leads to the following expressions for the buoyancy frequency and Rossby radius

$$N^2 = -\frac{g'}{H}\,, L_{R,n} = \frac{\bar{U}}{\pi f_0}, \tag{9}$$

where g' is the reduced gravity and $\bar{U} = \sqrt{g'H}$ is the velocity scale. When the width of the channel is comparable or larger than the Rossby radius of deformation, the effects of rotation are expected to be non-negligible.

III. Domain of Simulation and Computational Method

The domain of the simulation is illustrated in figure 1. An approximately two-layered flow moves into the domain from the inlet on the left side. A smooth increase in the depth of the lower layer is initially imposed, which will developed into a hydraulic jump as the simulation progresses. There is a topographic bump near the outlet on the right side, which transitions the flow to supercritical so disturbances do not

reflect off the outlet and propagate back into the domain. The top of the domain is approximated as a rigid lid because surface level variations are typically much smaller than the size of the internal hydraulic jump.

The governing equations are nondimensionalized using the upstream lower layer depth d_{1a} as the length scale, $\sqrt{g'd_{1a}}$ as the velocity scale, and $\sqrt{d_{1a}/g'}$ as the time scale. The two-layer Boussinesq limit of the problem can be fully described by four non-dimensional parameters in the frame of reference moving with the jump: the upstream lower layer velocity U_0, the upstream velocity difference between layers s, the total depth of the domain r^{-1}, and the lower layer downstream depth R [8], and they are nondimensionalized as

$$U_0 = \frac{u_{1a}}{\sqrt{g'd_{1a}}},\ s = \frac{u_{1a} - u_{2a}}{\sqrt{g'd_{1a}}},\ r^{-1} = \frac{D}{d_{1a}},\ R = \frac{d_{1b}}{d_{1a}}. \tag{10}$$

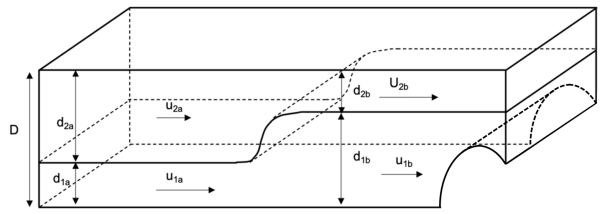

Fig. 1. Domain of simplified simulations

The domain is a rectangular channel and extends in the horizontal direction from $x = 0$ to $x = 16r^{-1}$, in the vertical direction from $z = 0$ to $z = r^{-1}$, and finally, in the transverse direction from $y = 0$ to $y = r^{-1}$. The topography near the outlet occurs well after the jump, and is therefore not shown in plots of the resulting flow. The simulation is initialized with a smooth transition region that develops into an internal hydraulic jump. The initial non-dimensionalized velocity field is given by

$$u(x, z, t = 0) = \frac{U_0}{d_1(x)} + \frac{\partial u(x)}{2}(1 - tanh[\lambda(z - d_1(x))]) \tag{11}$$

where $d_1(x)$ is the interface location and is given by

$$d_1(x) = 1 + \frac{R-1}{2}\left(1 + tanh\left[\frac{(x - x_0)}{L}\right]\right) \tag{12}$$

and $\partial u(x)$ is the velocity jump between the layers, given by

$$\partial u(x) = \frac{U_0}{d_1(x)} - \frac{(r^{-1} - 1)(U_0 - s)}{r^{-1} - d_1(x)} \tag{13}$$

with x_o marking the initial location of the imposed transition.

The initial density field is given by

$$b(x, z, t = 0) = \frac{1}{2}(1 - tanh[\lambda(z - d_1(x))]). \tag{14}$$

Simulation Name	f	R	r	s	U_0
rotation-b	0.025	3.4	0.1	1	2
rotation-c	0.05	3.4	0.1	1	2
rotation-d	0.1	3.4	0.1	1	2

TABLE I
PARAMETERS OF THREE-DIMENSIONAL SIMULATIONS

The initial vertical velocity has a no penetration boundary condition at the top and bottom of the domain, which are considered free-slip surfaces, and it satisfies the continuity equation within the interior. The inlet boundary conditions are defined by equations 11 and 14 evaluated at the position where $x = 0$. At the outlet of the domain, a Neumann condition is applied to the density and velocities with the pressure being hydrostatic. This allows the flow to propagate out of the domain. The topographic bump near the outlet transitions the flow back to supercritical, preventing waves from reflecting off the outlet boundary back into the domain. The refinement at the outlet of the domain is coarser with 64 cells in the vertical direction in order to diffuse waves ahead of the open boundary. The size of the time step is selected such that the CFL number is kept at a value no larger than 0.75 for all simulations. The viscosity ν and diffusivity κ are not defined explicitly for any of the simulations on the current work; instead, the code uses an implicit LES method wherein the numerical error associated with the computational scheme effectively parameterizes the turbulence.

The initial smooth transition develops into an internal hydraulic jump. Once the jump is fully developed, the time average of the flow can be analyzed. The jump front remains relatively stationary when compared to the simulation results of [8], but the reference frame is adjusted to account for movement of the jump, and the jump is analyzed in the frame of reference moving with the jump.

This work focuses on the results of three simulations with varying rotation rates, f. The simulations are summarized in table I, which shows the non-dimensional rotation rate, f, and the four non-dimensional parameters that fully describe a non-rotating internal hydraulic jump mentioned previously. For each simulation, the parameters other than the rotation are kept constant so the effect of rotation can be determined. The results for the 3D simulations are analyzed at different $x-z$ slices corresponding to different values of y, or positions across the width of the channel, because the flow is expected to vary across the transverse direction due to the effects of rotation.

IV. RESULTS AND DISCUSSION

A. Interface Height

As noted, the flow in each simulation is analyzed at three distinct locations across the length of the domain: $y = 2$, $y = 5$, and $y = 8$. These points correspond to locations near the side boundaries and at the centre of the channel because

previous work by Pratt [9] and Pratt et al [10] have shown that the behaviour of the flow varies across the width of the channel, and the properties of the hydraulic jump are expected to vary in the same direction due to the influence of rotation. The selected slices are chosen to represent the behaviour across the entire channel, which extends from $0 \leq y \leq 10$. However, a three-dimensional representation of the jump is also provided in Fig 2, which shows an isopycnal surface colored by the downstream flow velocity. The height of the downstream interface for a fully developed jump, $\tilde{R}(x)$, is used to conduct a qualitative analysis of the jump structure. The interface location is defined as

$$\tilde{R}(x) = \int_o^{r^{-1}} \frac{\rho(x,z) - \rho_{min}}{\rho_{max} - \rho_{min}} \, dz. \tag{15}$$

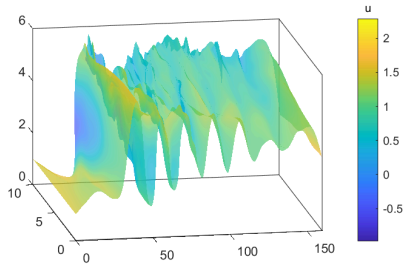

Fig. 2. 3D instantaneous hydraulic jump for $rotation\_d$ (with $f = 0.1$) at $t = 200$ (at the end of the averagving period). An isopycnal surface of $T = \frac{\rho - \rho_{min}}{\rho_{max} - \rho_{min}}$ is plotted, colored by the horizontal component of velocity, u.

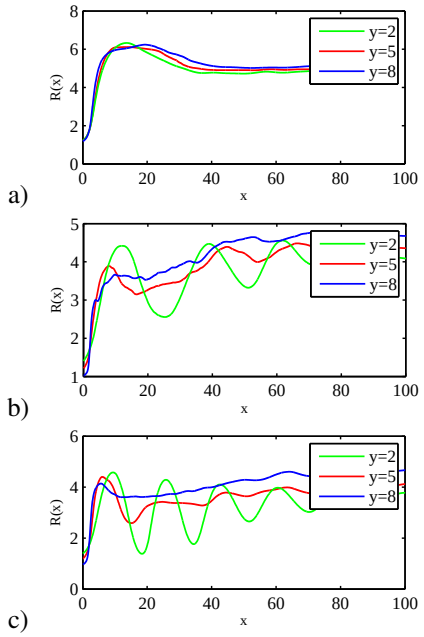

Fig. 3. Averaged interface heights along the channel for each of three positions across the channel width for a) rotation-b; b) rotation-c; c) rotation-d;

When analyzing the interface at the selected y positions, it is apparent that the flow banks towards the right side of the channel (for an observer looking in the direction of the flow), as expected for a flow in the northern hemisphere. The cross-channel variation in the lower layer depth upstream of the jump increases with the value of the rotation parameter f, with little change for the simulation with $f = 0.025$, and increasing variation as f increases to 0.05 and then 0.1. The height of the interface downstream of the jump also varies across the width of channel more significantly at higher rates of rotation, as shown in Fig 3. By taking an average of the interface height downstream of the jump for each cross-channel position, the difference in jump height across the width of the channel can be calculated (very small for $rotation\_b$ ($f = 0.025$), 0.610 for $rotation\_c$ ($f = 0.05$), and 0.894 for $rotation\_d$ ($f = 0.1$)). This difference in jump height variation across the width of the channel can be attributed solely to the increasing value of rotation since no other parameters have been changed in the simulations illustrated in Fig 3. Increasing the value of rotation results in more variation in the depth of the denser fluid upstream of the jump (and therefore in the lower layer upstream velocity as well), which results in a wider range of jumps heights across the width of the domain.

B. Qualitative Types of jumps

Ogden and Helfrich [8] identified four different qualitative types of jumps that may developed from flows with positive shear ($s > 0$; the expanding layer moves faster than the contracting layer), namely Undular Bores (UB), Smooth Front Turbulent Jumps (SFTJ), Fully Turbulent Jumps (FTJ), and Conjugate-state transitions (CS). The main characteristic of UBs is a train of solitary-like waves which decrease in amplitude until a uniform lower layer depth, which is larger than the upstream depth, is achieved; these jumps are also characterized by small amounts of mixing. The SFTJ presents as a smooth wave-like front with a small counter-clockwise recirculation region just downstream of the bore front, and a moderate amount of mixing is associated with these jump types. The FTJ features an overturning leading edge, and as in the case of the SFTJ, the region downstream of the bore front is fully turbulent with considerable amounts of mixing. CS transitions are smooth wave-like transitions which conserve energy across the jump.

In addition to the differences in the interface height across the width of the channel, the simulations in this work present several of these hydraulic jump structures. Distinct qualitative jump types may form at different positions across the width of the channel, within a single jump. The jump types are apparent in the time averaged density fields at different $x - z$ slice, shown in Fig 4. In $rotation\_b$ ($f = 0.025$), a SFTJ forms at $y = 2$, but the jump structure transitions to CS jump followed by a fully turbulent secondary jump by $y = 5$; this structure persists at $y = 8$. An UB with some shear instabilities at the interface forms along the right-most slice of the channel ($y = 2$) in $rotation\_c$ ($f = 0.05$); the jump

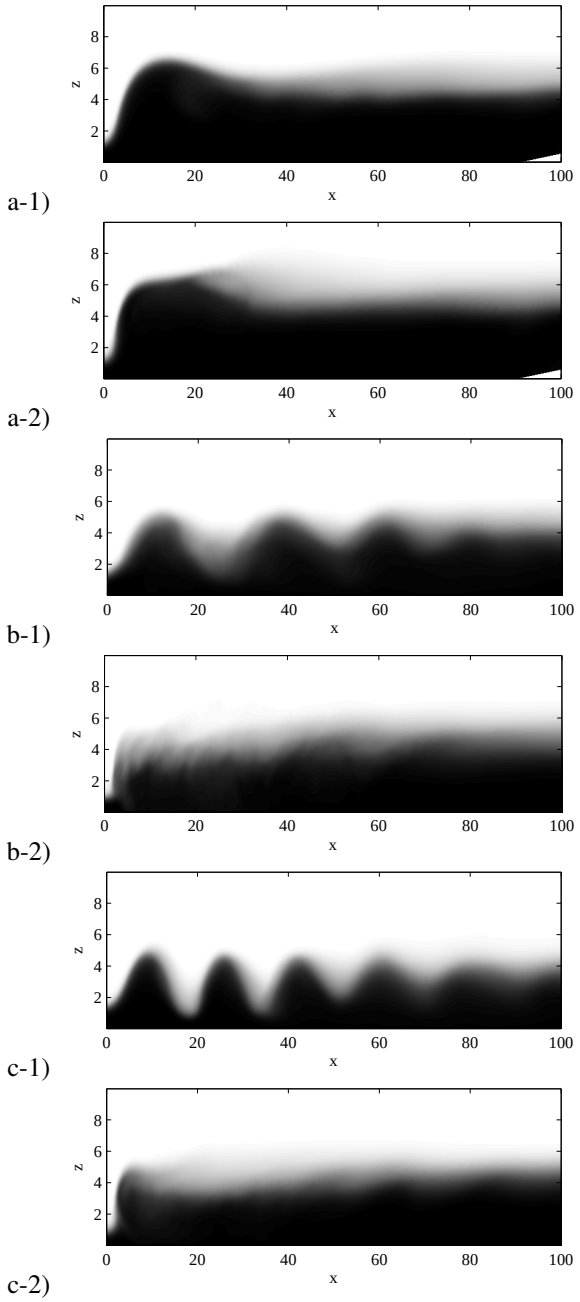

Fig. 4. Averaged density fields in x-z slice of domain. (a-) rotation_b ($f = 0.025$) averaged from $t = 300 - 351$; (b-) rotation_c ($f = 0.05$) averaged from $t = 300-350$; (c-) rotation_d ($f = 0.1$) averaged from $t = 100-200$. (-1) at $y = 2$; (-2) at $y = 8$.

structure transitions to a FTJ by $y = 5$, persisting at $y = 8$. In $rotation\_d$ ($f = 0.1$), an UB forms at $y = 2$, whereas the jump structure is a SFTJ at $y = 5$ and $y = 8$. The change in jump structure across the width of the jump can be explained by the variation in the upstream conditions across the width of the jump. Due to the changing upstream conditions, the jump height increases toward the left side of the channel (when looking in the direction of the flow), and the jump structure changes accordingly as described in the classification of jump structures by Ogden and Helfrich [8].

The shock joining theories discussed in [8] are used here to predict the jump height of the hydraulic jump at each position across the width of the domain. For each $x - z$ slice, the four non-dimensional parameters that describe the jump, r, s, U_0, and R are calculated and compared to the theoretical solution curve for specified r and s, which shows how the jump height R is expected to depend on the upstream lower layer velocity, U_0. Curves for each of three theories are shown; the theories differ by the layer in which energy is assumed to be dissipated. The simulation results are in reasonable agreement with the theories as presented for jumps with upstream shear by Ogden and Helfrich; for low values of shear (including all simulations discussed in detail here), larger jumps ($\bar{R} > 3$) were better predicted by the KRS theory (Fig 5).

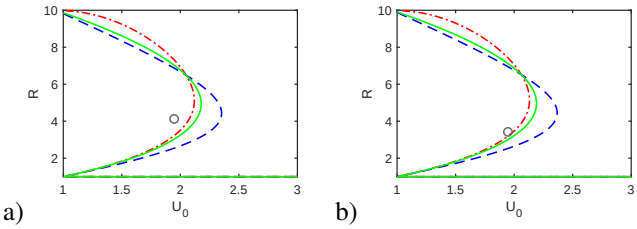

Fig. 5. Theoretical solution space and numerical simulation results at $r = 0.1$: a) $rotation\_c$; b) $rotation\_d$. $-\cdot-KRS$; $-VS$; $--WS$. Figures shows the jump analysed at $y = 2$.

C. Mixing

Identifying how the mixing of an internal hydraulic jump is affected by Earth's rotation is one of the main goals of this work. Turbulent mixing is one of the most important consequences of an internal hydraulic jump and it is responsible for dissipating energy in the flow and redistributing the fluid properties across the layers. The total amount of mixing is quantified here using the cumulative integral of the vertical component of the scalar variance production term in the turbulent scalar variance equation [7]:

$$P = \int_0^x \int_0^{r^{-1}} \overline{\mathrm{wT}} \frac{\partial \overline{T}}{\partial z} \, dz \, dx \qquad (16)$$

where $T = \frac{\rho - \rho_{min}}{\rho_{max} - \rho_{min}}$ is the turbulent fluctuation of the scaler (in this case density) and u is the turbulent velocity fluctuation.

This expression is used to calculate the amount of vertical mixing at each position across the width of the domain for each simulation. The cumulative integral of scalar variance production for different positions across the width of the domain is given on Fig 6. The cumulative integral of scalar variance is averaged in a region downstream of the jump to calculate a value representing the total mixing across the jump. This region is indicated with a grey bar in Fig 6. The values of P and the variation with position across the domain and with rotation rate are summarized on Fig 7, which shows that mixing increases to the left (when looking in the direction of

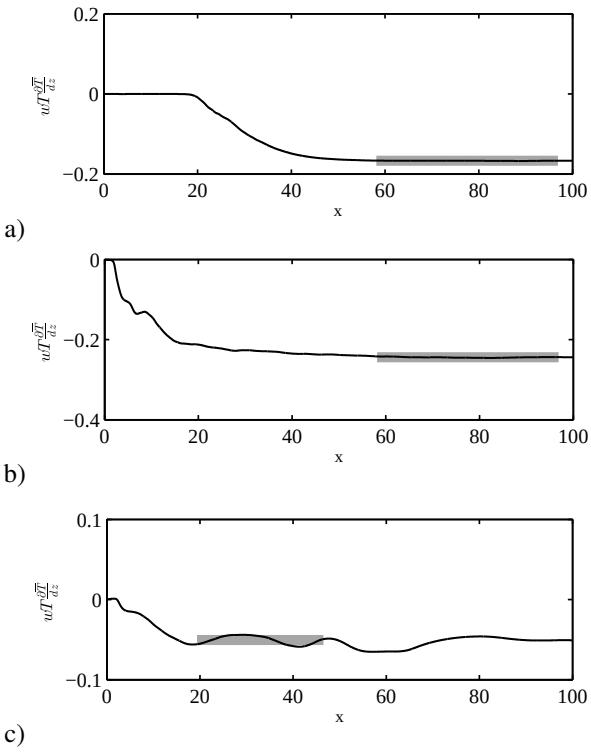

Fig. 6. Cumulative integral of the vertical component of scalar variance production, $wT\frac{\partial \overline{T}}{\partial z}$. (a-) rotation_b ($f = 0.025$); (b-) rotation_c ($f = 0.05$); (c-) rotation_d ($f = 0.1$), all for at $y = 8$. The gray bar indicates the values that are averaged to calculate the total mixing for the jump.

flow), and mixing decreases with increasing rotation. This is consistent with the smaller jumps and lower turbulence jump structures (UB vs. SFTJ or SFTJ vs. FTJ) that form closer to the right wall of the channel.

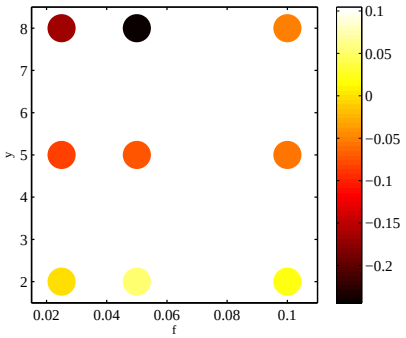

Fig. 7. Scalar Variance Production for different rotation parameters at different y values. On the x-axis: $rotation\_b$ ($f = 0.025$); $rotation\_c$ ($f = 0.05$); $rotation\_d$ ($f = 0.1$).

V. Conclusion

The effects of Earth's rotation on an internal hydraulic jump can be analyzed by considering the qualitative structure of the jump, how well the jump compares to existing two-layered theories, and how the mixing varies across the jump. The flow in the rectangular channel banks to the right with the difference in upstream lower layer depth across the width of the channel, which occurs and increases with rotation rate, resulting in different jump structures forming across the width of the channel. The amount of mixing varies across the width of the channel according to the qualitative jump type, with more turbulent jump structures producing more mixing. However, increasing the rotation rate reduces the amount of mixing. More simulations covering a wider range of values of rotation would help solidify these observations. The jump that forms at a specified position across the width of the channel (a specified y value) can be analyzed and compared to existing two-layered theories for jumps without rotation; however, it is important to understand how the jump's structure and mixing vary across the width of the channel. These results could be used to interpret observations that are frequently made along a single section (y value) of a channel.

References

[1] D. Farmer, and L. Armi, "Stratified flow over topography: the role of small-scale entrainment and mixing in flow establishment," Proc. R. Soc. Lond., vol.455, pp. 3221–3258, 1999.

[2] H. Chanson, "Current knowledge in hydraulic jumps and related phenomena. A survey of experimental results," European Journal of Mechanics - B/Fluids, vol.28, pp. 191-210, 2009.

[3] I. R. Wood and J. E. Simpson, "Jumps in layered miscible fluids," Journal of Fluid Mechanics, vol. 140, pp. 329–342, 1984.

[4] J. B. KLEMP, R. ROTUNNO, and W. C. SKAMAROCK, "On the propagation of internal bores," Journal of Fluid Mechanics, vol. 331, pp. 81–106, 1997.

[5] J. C. Sánchez-Garrido, G. Sannino, L. Liberti, J. García Lafuente, and L. Pratt, "Numerical modeling of three-dimensional stratified tidal flow over Camarinal Sill, Strait of Gibraltar," J. Geophys. Res., vol.116, 2011.

[6] J. M. Klymak and M. C. Gregg, "Three-dimensional nature of flow near a sill," Journal of Geophysical Research: Oceans, vol.106, pp. 22295-22311, 2010.

[7] K. A. Ogden, "Internal Hydraulic Jumps with Upstream Shear," Ph.D. dissertation, Join. Prog. in Phys. Oceanog., MIT, Cambridge, Massachusetts, 2017.

[8] K. A. Ogden, and K. R. Helfrich, "Internal hydraulic jumps in two-layer flows with upstream shear," Journal of Fluid Mechanics, vol. 789, pp. 64–92, 2016.

[9] L. J. Pratt, "On inertial flow over topography. Part 1. Semigeostrophic adjustment to an obstacle," J. Fluid Mech., vol. 131, pp. 195–218, 1983.

[10] L. J. Pratt, K.R. Helfrich, and E.P. Chassignet, "Hydraulic Adjustment to an Obstacle in a Rotating Channel," J. Fluid Mech., vol. 404, pp. 117–149, 2000.

[11] M. Gregg, and L. J. Pratt, "Flow and Hydraulics near the Sill of Hood Canal, a Strongly Sheared, Continuously Stratified Fjord," Journal of Physical Oceanography, vol.40, 2010.

[12] M. Li and P. F. Cummins, "A note on hydraulic theory of internal bores," Dynamics of Atmospheres and Oceans, vol.28, pp. 1 - 7, 1998.

[13] P. F. Cummins, L. Armi, and S. Vagle. "Upstream Internal Hydraulic Jumps," Journal of Physical Oceanography, vo.36, pp. 753-769, 2006.

[14] S. A. Thorpe and L. Li, "Turbulent hydraulic jumps in a stratified shear flow. Part 2," Journal of Fluid Mechanics, vol. 758, pp. 94–120, 2014.

[15] S.A. Thorpe, J. Malarkey, G. Voet, M.H. Alford, J.B. Girton, and G.S. Carter, "Application of a model of internal hydraulic jumps," J. Fluid Mech., vol.834, pp. 125–148, 2018.

[16] S. Popinet, "Gerris: A tree-based adaptive solver for the incompressible Euler equations in complex geometries," Journal of Computational Physics, vol.190, pp. 572-600, 2003.

[17] K. A. Ogden, and K. R. Helfrich, "Internal hydraulic jumps in two-layer flows with increasing upstream shear," Physical Review Fluids, vol. 5(7), 2020.